AIRFLOW CHARACTERISTICS OF A SPRAY UAV AND ITS EFFECT ON SPRAY DROPLET TRANSPORTATION

Shilin Wang[1], David Nuyttens[2], Daipeng Lu[1], Jonathan Van Beek[2], Xue Li[1*]

[1*]Corresponding author. Institute of Agricultural Facilities and Equipment, Jiangsu Academy of Agricultural Sciences, Nanjing, China.
E-mail: neigelee99@163.com | ORCID ID: https://orcid.org/0009-0003-3723-0002

ABSTRACT

To explore the downwash airflow characteristics of a multi-rotor UAV and its effect on droplet movement and deposition, a comparative experiment between static-state and hovering-state spraying was carried out with a DJI MG-1P eight-rotor plant protection UAV. The results showed that the overall strength of the downwash airflow decreased further below the UAV. The direction of the airflow directly under the UAV was almost vertically downward and first increased and then decreased in speed. Closer to the ground, the airflow was directed outward with angles in the vertical direction of 71.3° and 81.5°. In general, the downwash airflow velocity and direction on both sides of the UAV were nearly symmetrically distributed. Compared with the static-state spraying, the high-speed downwash airflow in the hovering-state spraying significantly increased droplet velocity and size. The downwash airflow increased the amount of spray deposition in the different measurement layers but reduced the uniformity of the deposition. For the section (L-B-F-J-M) perpendicular to the flight direction, the near ground deposition was the best for the hovering-state spraying, with an average deposition of 5.85 μL/cm^2 and an *RSD* of 36.87%. This study can be a reference for the optimization of the downwash airflow and the improvement of the spray application uniformity of multi-rotor UAVs.

INTRODUCTION

In recent years, the low altitude and low volume application of plant protection products (PPP) using an Unmanned Aerial Vehicle (UAV) has received extensive attention and achieved comprehensive development (Li et al., 2021; Pinguet, 2021; Kumar et al., 2022). The number and use of UAVs for plant protection is growing rapidly (Hafeez et al., 2022), which has effectively solved the bottlenecks of low operating efficiency and poor applicability of ground based PPP application in paddy fields and hilly mountains (Lan & Chen, 2018; Xiongkui et al., 2017). Different from traditional ground sprayers, the rotors of a plant protection UAV provide the necessary lift for the UAV body while the downwash airflow below the body can theoretically form an air-assisted spray effect (Giles & Billing, 2015; Li et al., 2018).

In order to accurately obtain the spatial distribution of the downwash airflow under a UAV, Hu et al. (2014) designed a wireless sensor network measurement system for a real-time acquisition of an UAV airflow field in multiple points and directions. Li et al. (2019) designed a three-dimensional airflow measurement platform to acquire the vertical distribution and vortex structure of the rotor airflow field. In addition, it has become a mainstream method to study the characteristics of a UAV airflow field using numerical simulations. In order to clarify the spatiotemporal distribution of the air flow field of a UAV, Zhang et al. (2020b) adopted the lattice Boltzmann method (LBM) to simulate the airflow field of a six-rotor spray UAV based on a mesoscopic kinetic model. Yang et al. (2017) and Zhang et al. (2017) combined Navier Stokes equations with k-ω Turbulence model to numerically simulate the downwash airflow of a single rotor and six rotor spray UAV. Teske et al. (2018) summarized the ability of two models to predict spray drift and deposition from rotary wing spray UAVs. Zhang et al. (2021)

[1] Institute of Agricultural Facilities and Equipment, Jiangsu Academy of Agricultural Sciences, Nanjing, China.
[2] Flanders Research Institute for Agriculture, Fisheries and Food (ILVO), Merelbeke, Belgium.

established a set of motion equations by analyzing the force on droplets in the UAV airflow field and designed an equation solving program using Matlab software to realize the iterative calculation of droplet speed, displacement and other parameters. The results showed that the downwash UAV airflow field is the main factor affecting the final droplet velocity. Although these studies have analyzed the downwash UAV airflow field and the final settling velocity of droplets, the air distribution profile and the motion characteristics of droplets during the settling process were not considered.

To explore the influence of the UAV airflow field on droplet deposition and distribution, researchers conducted a large number of field experiments. Wang et al. (2018a) tested the airflow velocity and droplet distribution under spray UAVs based on the spatial mass balance method, and found that the airflow distribution of the UAVs rotor is closely related to the droplet deposition. Lan et al. (2021) compared the effect of flight parameters of multi rotor UAVs on droplet deposition, and found that the downwash airflow field is the most important factor affecting droplet deposition and distribution. Chen et al. (2017a; 2017b) used the UAV rotor airflow field measurement system to study the influence of the airflow field of single and multi-rotor UAVs on aerial spray droplet deposition. The mechanism of the influence of the airflow field under the UAV rotor on droplet distribution in the air was revealed, providing guidance to reduce spray drift and improve PPP use. Wang et al. (2020) compared the influence of the downwash airflow field of an eight rotor UAV on droplet deposition distribution for different flight parameters. The results showed that the downward airflow improves droplet sedimentation. When the flight speed is between 1.0 m/s and 3.0 m/s, droplet deposition had a very significant positive correlation with downwash airflow intensity. In addition, Shi et al. (2021) analyzed the impact of the downwash airflow of a multi rotor UAV on the dynamic behavior of rice plants, and found that the larger the downwash airflow, the more obvious the deformation of rice plants. The canopy morphology of the plant strongly affects droplet deposition. Tang et al. (2017)

used a high-speed particle imaging velocimetry system to test the movement and deposition behavior of spray droplets under an eight rotor UAV at different rotation speeds. The results showed that the downwash airflow speed not only affects the spray deposition but also the spray distribution uniformity.

The above studies have shown that the airflow field generated by the rotors of a spray UAV affects the movement behavior of spray droplet and the resulting spray deposition and distribution. It is therefore important to further investigate the influence of the rotor airflow field of the spray UAV on spray behavior to improve the deposition of spray droplets on the target, improve the spray uniformity and reduce the drift risk (Zhang et al., 2020a; OECD, 2021). Among the various models of spray UAVs, multi-rotor UAVs are most common, due to their advantages such as light weight, flexible operation and stable flight (Wang et al., 2018b). Therefore, this study measured the downwash airflow characteristics of an eight-rotor spray UAV. The effect of the downwash airflow on spray droplet movement and deposition was carried out in a comparative experiment between static state and hovering state spraying.

MATERIAL AND METHODS

Eight rotors plant protection UAV

A DJI MG-1P eight-rotor spray UAV was taken as the research object. The symmetrical motor wheel base of the UAV is 1.5 m, the single arm length is 0.619 m, the rotor diameter is 0.543 m, and the fuselage width when the arm is extended is 1.460 m (excluding the rotor). A picture and aerodynamic layout of the UAV is shown in Figure 1. The system is composed of four main booms in "X" layout. The outer end of each main boom is extended into a "Y" secondary boom. The main and secondary booms form an eight-rotor system with a symmetrical structure. Eight symmetrically arranged brushless motors power their corresponding rotors. The flight control system controls the rotation speed and direction of each rotor to jointly provide the upward lift for the frame.
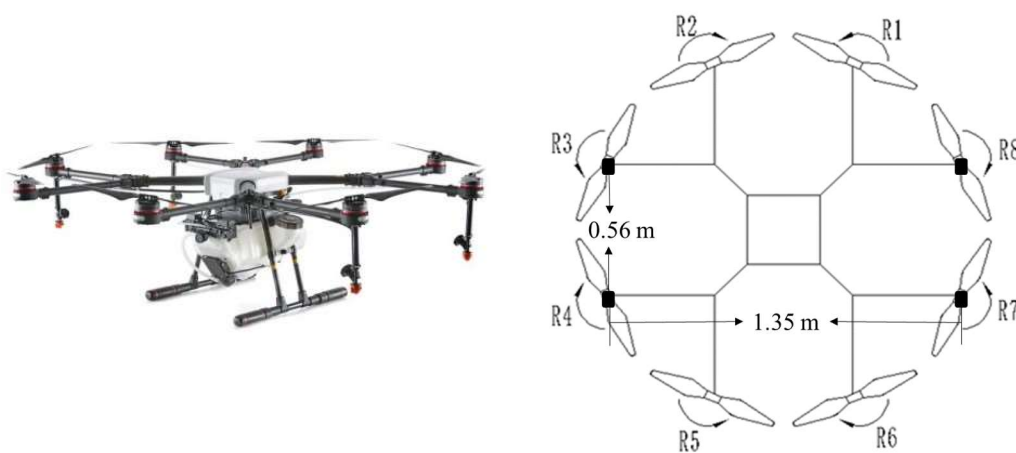
FIGURE 1. Picture (left) and aerodynamic layout (right) of the eight-rotor DJI MG-1P plant protection UAV.

The UAV generates a different lift by adjusting the rotation speed of each rotor in order to adjust its flying attitude. In hovering state, the eight rotors of the UAV rotate at the same speed, but the adjacent rotors turn in opposite directions. In Figure 1, R1 and R2 are the nose of the UAV, R5 and R6 are the tail of the UAV. The motors of R1, R3, R5 and R7 rotate counterclockwise while the motors of R2, R4, R6 and R8 rotate clockwise. An XR110 01 VS flat fan spray nozzle (TeeJet Technologies, USA) is mounted 0.33 m below rotors R3, R4, R7 and R8. The distance between nozzles on the same side of the UAV fuselage is 0.56 m, and the distance between nozzles on both sides of the fuselage is 1.35 m (Figure 1). The main parameters of the eight-rotor plant protection UAV are shown in Table 1.

TABLE 1. Basic technical and spraying parameters of the tested UAV.

Item	Parameters	Item	Parameters
UAV Model	DJI MG-1P	Nozzle type	XR11001VS
Overall dimensions (m)	1.46×1.46×0.58	Nozzles	4
Maximum flying speed（m/s）	7	Droplet diameter （μm）	130～250
Tank volume (L)	10	Spraying swath （m）	4～6

Downwash airflow measurement

The downwash air flow field of the DJI MG-1P UAV in hovering state was measured using a 3D anemometer (WindMaster Pro, Gill, UK) connected to a SP500 data logger (LSI LASTEM, Italy). The 3D anemometer provides air speed and direction data with 3-vector outputs (U, V, W). The air speed measurement range is 0-65 m/s with a resolution of 0.01 m/s. The airflow direction measurement range is 0-359 °with a resolution of 0.1°, and the maximum output frequency is 32 Hz.

In order to avoid the disturbance of natural wind on the test results, the test was performed at a flat ground (20 m × 30 m) surrounded with buildings with a height 5 m and all tests were performed in windless weather. During the experiment, the hovering height of the UAV was set 2.3 m. A cube metal frame with a side length of 2 m was placed directly below the UAV body as the downwash airflow experiment measuring area. The measuring points were spatially divided according to Figure 2. Five horizontal cross sections were selected as shown in Figure 2a at different distances below the UAV body and labeled $L_1 \sim L_5$ from high to low. Section L_1 was located 50 cm below the airframe (D_l=50 cm), and the distance between adjacent measurement sections was 40 cm. In each section, a total of 13 measuring points were selected, A_i, B_i, C_i, ..., M_i (i is the section number), as shown in Figure 2b, where F_i was the central point (directly below the fuselage) of the measurement section, H_i was the nose direction of the UAV, and D_i was the tail direction of the UAV. The distance between sampling points L_i, B_i, F_i, J_i and M_i was 0.5 m as well as the distance between sampling points D_i, E_i, F_i, G_i and H_i.

The anemometer sensor was placed horizontally at each measurement point. When one measurement point was completed, the sensor was moved to the next point. The sampling frequency of the 3D anemometer was set at 1 Hz. Each sampling point was measured three times to determine the average value, and the duration of each measurement was 30 s.
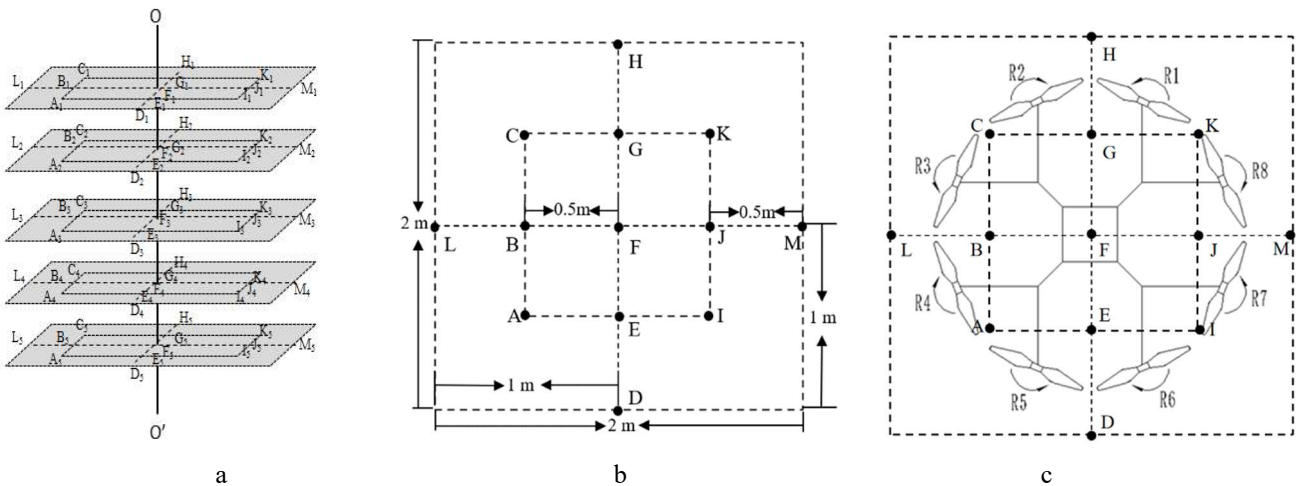
FIGURE 2. Sampling diagram of downwash airflow experiment: a. Schematic of the horizontal measurement layers; b. Measurement points arrangement; c. Relative position of the UAV above the measurement points.

Measurement of droplet size and velocity distribution

The effect of the downwash airflow on spray droplet size and velocity characteristics was determined by measuring droplet sizes and velocities when the UAV rotor was both stationary and hovering at a spray pressure of 0.3 MPa. A particle droplet image analyser (PDIA) system (VisiSize P15, Oxford Lasers, UK) was used to determine the droplet size and velocity distribution (Kashdan et al., 2007; França et al., 2018). Since the altitude of the hovering UAV was 2.3 m, a metal truss was used to fix the UAV at a height of 2.3 m during the experiment with a stationary rotor. The PDIA measuring points were consistent with Figure 2. A small lift table was used to carry the PDIA system to different measurement heights.

In order to ensure the accuracy of the measurements, the pulse interval of the PDIA was adjusted in order to guarantee a reliable droplet velocity calculation. PDIA settings resulted in a droplet size measuring range from 10 µm -1000 µm and a droplet velocity range from 0 m/s -15 m/s. Droplets with a sphericity below 0.7 or at the image boundary were excluded. Each sampling point was measured three times with a measuring time of 10 s.

Measurement of spray distribution

In order to explore the influence of downwash UAV airflow on the spray distribution, the spray deposition at each sampling point was measured at a spray pressure of 0.3 MPa when the UAV rotor was both stationary and hovering. The way of mounting the UAV for the stationary rotor experiment was consistent with the droplet size and velocity measurements, and the spray deposition sampling points were consistent with Figure 2.

The cube metal frame used for the airflow measurement was also used to fix disposable petri dishes (d=90 mm) with aluminium beams to collect settling droplets and measure spray deposition. Each measurement was conducted for a single measurement layer to avoid the interference of petri dishes and aluminium beams of other layers. The duration of each measurement was 10 s with 3 repetitions.

Allure Red 85 (Shanghai Dyestuff Research Institute Co., Ltd.) was used as a tracer in the spray solution at a mass concentration of 2 ‰. After the spray experiment, deionized water was added to elute the petri dishes. A 722s ultraviolet visible spectrophotometer (Shanghai Yidian Analytical Instrument Co., Ltd.) was used to measure the absorption value of the eluent at 501 nm. According to ISO 24253 (2015), the spray deposition per unit area at each sampling point was calculated according to [eq. (1)].

$$\beta_{dep} = \frac{(\rho_{smpl} - \rho_{blk}) \times F_{cal} \times V_{dil}}{\rho_{spray} \times A_{col}} \quad (1)$$

With:

β_{dep} the spray deposition per unit area (mL/cm^2);

V_{dil} the volume of added eluent (mL);

ρ_{smpl} the absorption value of the eluent (-);

ρ_{blk} the absorption value of the eluant of blank Petri dishes;

ρ_{spray} the mass tracer concentration in the spray solution (g/L);

F_{cal} the relationship coefficient between absorption value and tracer concentration (µg/L),

A_{col} the area of petri dish collector (cm^2).

In order to evaluate the homogeneity of the spray deposition in the same layer, relative standard deviation (*RSD*) was calculated as the ratio between the standard deviation of spray deposition values at the different sampling points (in the same layer) to the mean spray deposition value in that layer. The lower the *RSD*, the more uniform the spray distribution in one layer. The calculation method is shown in [eq. (2)].

$$RSD = \frac{\sqrt{\frac{\sum_{i=1}^{n}(X_i - \bar{X})}{n-1}}}{\bar{X}} \times 100\% \quad (2)$$

With:

X_i the spray deposition value of the *i*-th sampling point;

$\bar{X}$ the mean spray deposition over all sampling points, and

n the total number of sampling points.

Statistical Analysis

The droplet velocity and volume median diameter of measurement points in the same test layer were analyzed with a factorial analysis of variance (ANOVA). The significance of the differences were evaluated by Duncan's test for a significance level of 95%. All the analyses were performed with the statistical software SPSS v.19.0 (SPSS Inc., Chicago, IL, USA).

RESULTS AND DISCUSSION

Downwash air flow

Figure 3 shows the downwash air velocity distribution created by the rotors in different measurement layers under the UAV. Due to the great difference in airflow velocities among the measurement layers, different scales were used to visualize the airflow distribution in each layer Central sampling point F, which was directly below the UAV fuselage, was taken as the origin with the direction of the UAV nose (points G and H) at 0 °. At 50 cm below the UAV, the air velocities where highest in a circular area from 40 to 60 cm from point F with an average air velocity in this area of about 8 m/s. Due to the blocking effect of the UAV fuselage on the airflow, the air velocity near point F was low with an average value of only 1.12 m/s.

With the increase of the distance below the UAV, the downwash velocity distribution becomes more diffuse. At distances from 90 cm to 170 cm below the UAV, highest air speeds are found in the circular region from 10 cm to 70 cm from point F. Meanwhile, the downwash

airflow intensity decreased slightly with an increasing distance below the UAV with maximum air speeds of 7.75 m/s, 6.95 m/s and 6.50 m/s at distances of 90 cm, 130 cm and 170 cm below the UAV.

At the distance of 210 cm below the UAV (or 20 cm above the ground), the core area of the downwash airflow of the UAV rotor further diffused to the periphery of the measuring area due to the blocking effect of the ground. In this layer, air velocities at the different sampling points were relatively uniform with an average of 3.24 m/s and highest values of about 4 m/s on the left and right side of the UAV fuselage.
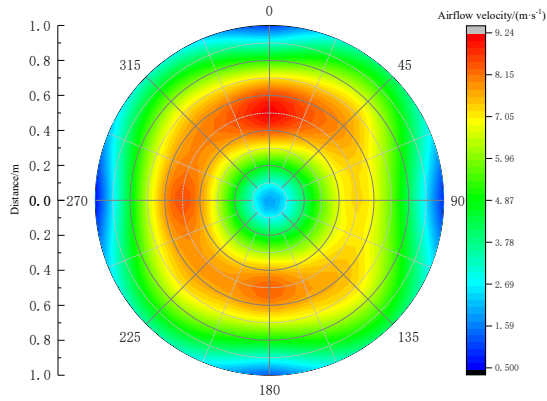
a. D_1=50 cm below the UAV
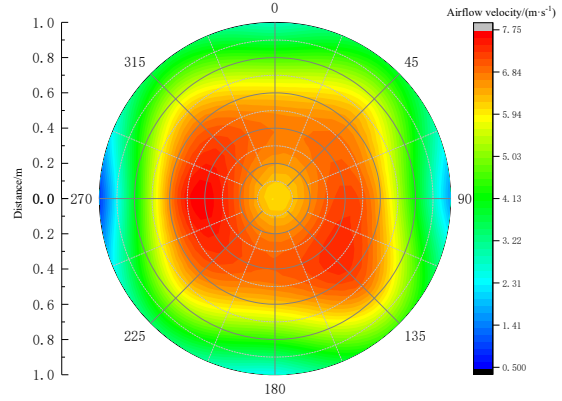
b. D_2=90 cm below the UAV
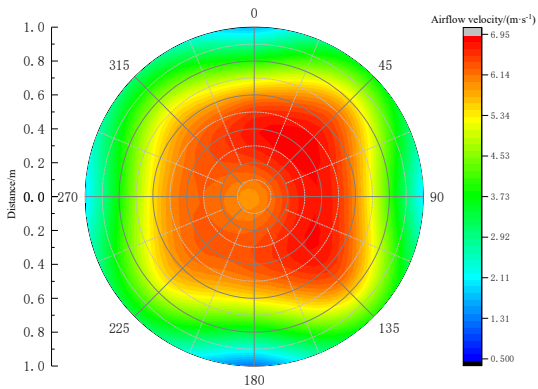
c. D_3=130 cm below the UAV
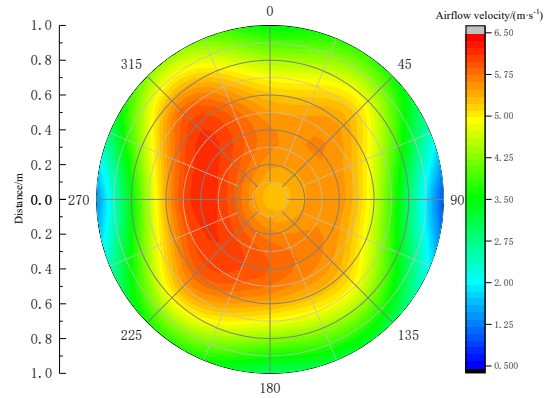
d. D_4=170 cm below the UAV
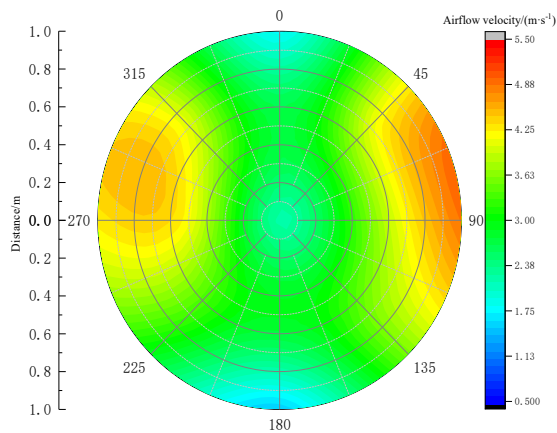
e. D_5=210 cm below the UAV
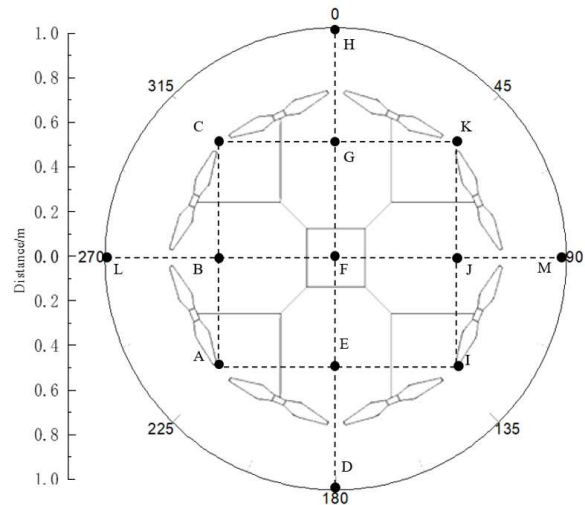
f. Relative position of the UAV

FIGURE 3. Downwash air velocity distribution at different measurement layers under the UAV (a-e) and the relative position of the UAV above measurement layers (f).

In order to visualize the downwash airflow speed and direction of the UAV rotor, the vertical section composed of sampling points L, B, F, J and M in the different layers was selected to present the downwash airflow distribution vector diagram (Figure 4). In the figure, only the vertical and the lateral airflow velocity was considered, and the longitudinal airflow was ignored. The results confirm that the air velocity at point F increased first and then decreased with an increasing distance from the UAV resulting in a lower air velocity in point F in the top and bottom layer compared with the three middle layers. Meanwhile, the air velocity of the middle three layers decreased with an increasing distance below the UAV. The air velocities at points B and J (on the left and right sides of the UAV fuselage) were significantly higher than that in other points. Air velocities at points L and M (on the outsides of the UAV fuselage) were always the lowest except for the measurement layer close to the ground due to the blocking effect of the ground.

The air flow direction in point F directly below the UAV fuselage was approximately vertically downward, while the air flow direction in the areas on both sides of the UAV fuselage was in the shape of a horn which "contracts first and then expands". This experiment result is consistent with the simulation result of Yang et al. (2018) based on a three dimensional CFD model. At 50 cm below the UAV, the downward air flow in points L and M inclined to the center of the measurement area, and the included angle with the vertical direction was 43.6° and 49.2°, respectively. At 20 cm above the ground, the downward air flow in points L and M inclined to the outside of the measurement area with included angles of 71.3° and 81.5°, respectively. Overall, the air velocity and direction of the downwash airflow on both sides of the UAV fuselage are symmetrically. Spray droplet trajectories are determined both by the position of nozzles and the downwash airflow distribution (Herbst et al., 2020; Tang et al., 2017). Therefore, the position of the nozzles mounted on the UAV can be optimized knowing the downwash airflow pattern, which is of great significance to reduce aerial spray drift and increase the deposition in the target area.
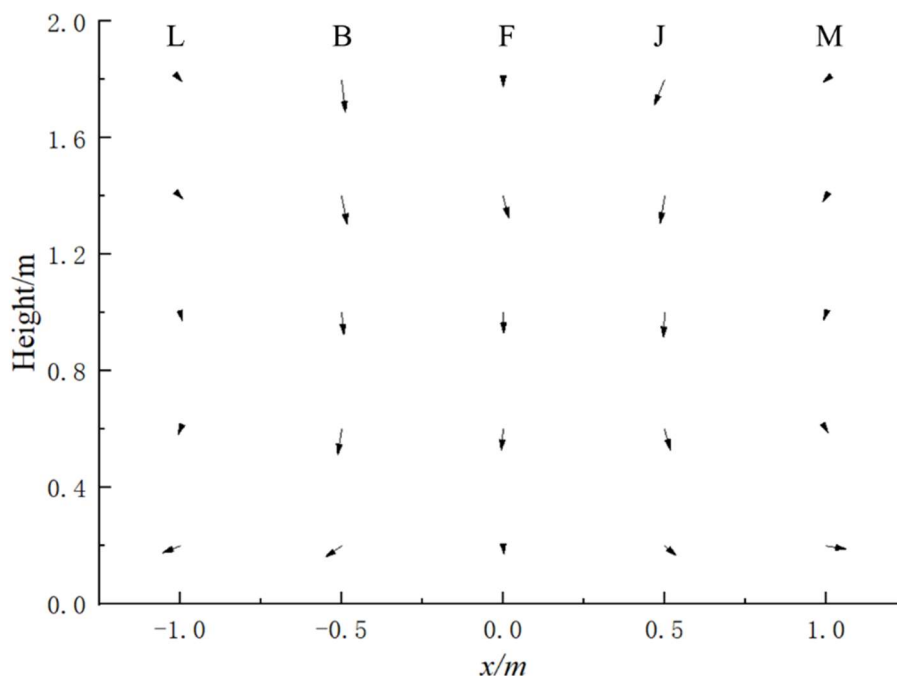
FIGURE 4. Vector diagram of downwash airflow distribution in L-B-F-J-M section.

Droplet size and velocity distribution

The spray droplet velocity distribution at the different sampling layers and positions is shown in Table 2. Because the direction of the spray fans of the four nozzles was perpendicular to the direction of the UAV nose, no spray droplets were detected when the UAV rotors were stationary in points D and point H in layer L_1. With an increasing distance below the nozzle and UAV, the spray area of the nozzles further diffused, and part of droplets moved obliquely towards the nose and tail area of the UAV. Therefore, droplets were also detected at points D and H in layers L_2 to L_5 during static-state spraying. However, during hovering-state spraying, the downwash airflow generated by the high-speed rotation of the UAV rotors clearly affected the movement and spatial distribution of the droplets (Li et al., 2018; Zhang et al., 2020b). Tang et al. (2017) also found that the UAV rotor downwash airflow reduces the spray angle of the nozzle. This decrease in spray fan angle results in a narrower spray area. Consequently, droplets were not detected at multiple sampling points. The closer to the nozzles and UAV the higher the number of sampling points without detected droplets.

During static-state spraying, the settling velocity of the spray droplets was slow, with all values below 1 m/s. In layer L_1, the maximum droplet velocity was 0.48 m/s in point J while the lowest droplet velocities were measured under the UAV fuselage at points E, F and G with values around 0.2 m/s. The droplet velocities in the L-B-F-J-M section of layer L_3 ranged from 0.68 to 0.87 m/s without significant differences among the sampling points, while the velocities of these points were significantly higher than those of the other points in the same layer. The droplet velocity distribution in layers L_4 and L_5 showed a similar

pattern as layer L_3. During static-state spraying, the droplet velocities of L_3, L_4 and L_5 layers showed an increasing trend. Droplet velocities at the different sampling points of L_5 layer were quite uniform probably because they reached a constant settling state at that height.

The movement characteristics of the droplets changed significantly in hovering-state under the influence of the downwash airflow (Sun & Liu, 2019; Xiahou et al., 2020; Zhang et al., 2021). Spray droplet velocities in hovering state were all much higher than in stationary state at the same sampling point. Average droplet velocities at point B and J of layer L_1 were 8.6 m/s and 10.3 m/s, respectively. The droplet velocity at point F directly below the fuselage was only 3.0 m/s, which was highly consistent with the downwash airflow characteristics shown in Figure 3a. Also for the layers L_2 to L_5, average droplet velocities were generally consistent with the downwash airflow velocities of the corresponding layer.

TABLE 2. Droplet velocity distribution (m/s) on different measurement layers and sampling positions.

Sampling points	Static state					Hovering state				
	L_1	L_2	L_3	L_4	L_5	L_1	L_2	L_3	L_4	L_5
A	0.34ab	0.25c	0.26b	0.66abc	0.77a	--	8.9a	3.4e	--	5.4abc
B	0.34ab	0.36bc	0.87a	0.84a	0.78a	8.6a	8.8a	7.2bc	4.9cd	6.3a
C	0.26bc	0.29c	0.30b	0.72ab	0.76ab	--	7.7ab	7.9abc	6.6ab	4.7bcd
D	--	0.22c	0.25b	0.34e	0.39d	--	--	--	--	--
E	0.22bc	0.36bc	0.30b	0.48cd	0.68abc	--	7.4ab	--	--	4.5bca
F	0.21bc	0.36bc	0.76a	0.58bcd	0.64bc	3.0b	6.5b	8.3ab	7.3a	4.0cd
G	0.16c	0.35bc	0.25b	0.55bcd	0.58c	--	--	6.6cd	--	4.7bcd
H	--	0.28c	0.12b	0.45de	0.57c	--	--	--	--	--
I	0.16c	0.51ab	0.19b	0.58bcd	0.66abc	--	7.8ab	8.8a	4.3d	5.8ab
J	0.48a	0.54a	0.69a	0.64abc	0.45d	10.3a	7.1ab	9.0a	5.8bc	5.5ab
K	0.20bc	0.61a	0.15b	0.44d	0.61c	--	3.4c	5.4d	5.1cd	5.8ab
L	0.37ab	0.51ab	0.84a	0.82a	0.68abc	3.8b	3.3c	3.3e	5.1cd	3.3de
M	0.17c	0.50ab	0.71a	0.65abc	0.76ab	1.3b	1.9c	2.1e	1.7e	2.4e

Note: --: represents no droplet was detected; data in table are the average of three replicates. Different letters in the same column indicated significantly different at P<0.05 level. Similar for Table 3.

In general, droplet velocities decreased going from layer L_1 to L_5 which is in agreement with the downwash airflow results. Due to the shelter effect of the UAV fuselage, droplet velocity at point F first increased and then decreased with velocities of 3.0 m/s, 6.5 m/s, 8.3 m/s, 7.3 m/s and 4.0 m/s for layers L_1 to L_5. For all layers, droplet velocities at points L and M were generally the lowest because of their location at the edge of the sampling and downwash airflow area. The UAV was not completely stable during hovering-state spraying, but tilted or skewed at the center position, resulting in different droplet velocities of the symmetrical points L and M. These results are again in line with the downwash airflow characteristics (Figure 4).

Due to the effect of the downwash airflow on droplet trajectories, only for layer L_5 (at 210 cm below the UAV) a complete droplet velocity polar coordinate contour diagram can be obtained (Figure 5). It is clear that the droplet setting velocity in hovering state was significantly greater than in static state. It is worth mentioning that the droplet velocity in hovering state was slightly higher than the corresponding airflow velocity shown in Figure 3e, which may be due to the fact that the droplets had a greater inertia under the transport of the upper airflow, so the droplet velocity was closer to the airflow velocity of layer L_4 (Figure 3d). Meanwhile, droplets with higher velocity in hovering state were mainly concentrated in the area directly below the nozzles (Figure 2c), and the droplet velocity distribution of the 4 nozzles of the UAV were basically the same. In contrast, the droplet velocity in static state was not affected by the rotor airflow and was more conducive to outward diffusion. Therefore, the difference in droplet velocities in layer L_5 in static state was small.

a. Static state   b. Hovering state
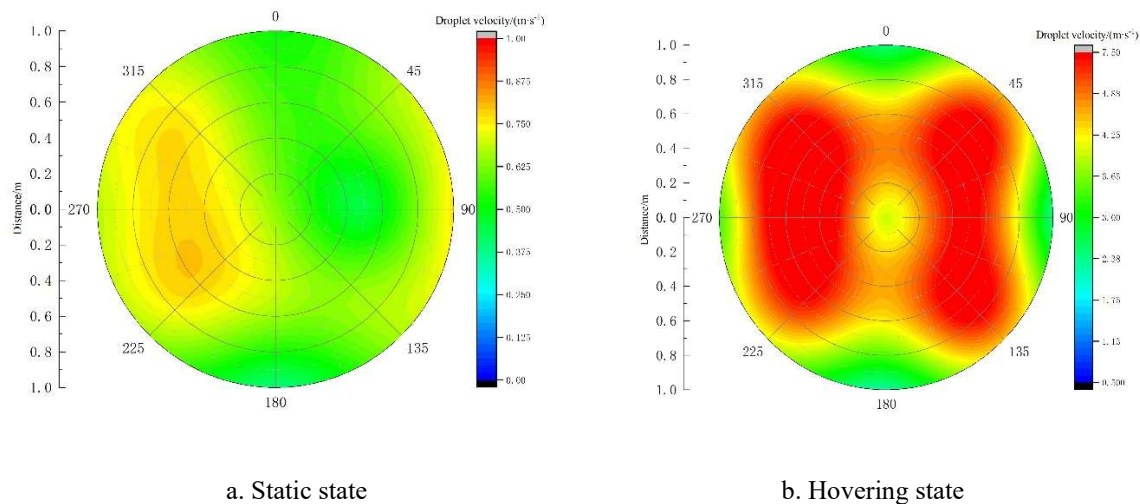
FIGURE 5. Droplet velocity distribution at 210 cm below (layer L_5) the UAV.

Spray droplet size results, expressed as volume median diameter (VMD), at different sampling layers and positions are shown in Table 3. In static state, smallest VMD values are found at points D and H which are the sampling positions furthest away from the nozzles. VMD values at points D and H ranged from 50 to 60 μm in layers L_2 to L_4 with the exception of point H in L_4 (VMD = 74.4 μm). In layer L_5, VMD values at points D and H increased to 93.9 μm and 94.0 μm, respectively. This might be caused by the outward diffusion of larger droplets from the central spray area near the ground.

In static state, VMD values at the central F position from layer L_1 to L_5 were 82.3 μm, 132.0 μm, 131.2 μm, 145.1 μm and 151.8 μm, respectively. The droplet sizes in point F from layers L_2 to L_5 were relatively larger than that of L_1 layer. Similar results were found at positions L and M, with low VMD values in layer L_1 (80.0 μm and 66.4 μm) and higher VMD values (generally > 115 μm) in layers L_2 to L_5. Wang et al. (2015) evaluated the droplet size distribution of standard flat fan nozzles, and found that the droplet size at the periphery of the spray fan was larger than at the centre of the fan. In this study, points F, L and M are located at the margins of the spray fans. The low VMD values at these positions in layer L_1 can be explained by the fact that the spray fans are hardly reaching these positions in layer L_1, so only some small swirling droplets are measured.

In hovering-state, no droplets were in several sampling points due to the downwash airflow. In points D and H, no droplets were detected in any of the measurement layers. At the positions where droplets were detected, the VMD values were significantly higher in hovering state compared with the corresponding values in static state with VMD values ranging from about 150 μm up to 200 μm and above. The atomization of droplets is driven by the shear force between the liquid sheet and the ambient air. The stronger the shear force, the ampler the atomization effect (Reitz & Bracco, 1982). Using an electric backpack sprayer, Wang et al. (2016) found that the airflow generated by the electric fan directly behind the nozzle could significantly increase its spray droplet size distribution. In this study, the rotor airflow of the UAV was coincident with the spray direction of the nozzles, so it was speculated that the high-speed downwash airflow generated by the rotors weakened the shear force between the air and the liquid sheet, resulting in the larger droplet size in the hovering-state spraying.

Similar to static-state spraying, droplet sizes in hovering state in the margins of the spray fans (points F, L and M) were larger with generally values above 200 μm. However, for points L and M, VMD values decreased in layer L_4 to 181.8 μm and 194.3 μm, and then further decreased to 151.1 μm and 193.9 μm in layer L_5. As shown in Figure 4, the airflow starts to diffuse to the periphery starting from layer L_4, which forces the smaller droplets in the internal area of the spray fan to move to points L and M, resulting in the decrease in VMD values.

During pesticide application, droplets impacting on the target surface will spread to the maximum diameter and then shrink eventually forming bouncing, shattering or retention (Zwertvaegher et al., 2014; Weisensee et al., 2016). Whereas, only droplets retained on the target can exert its biological efficacy (Boukhalfa et al., 2014). The impaction outcomes of droplets mainly depend on its diameter, velocity, and physicochemical properties (Nairn & Forster, 2014). According to the changes of the droplet size and velocity under the downwash airflow, the nozzle and spray parameters of UAVs can be adjusted to enhance the adhesion rate of droplets on the targets.

TABLE 3. Volume median diameter (μm) of droplets on different measurement layers and sampling positions.

Sampling points	Static state					Hovering state				
	L_1	L_2	L_3	L_4	L_5	L_1	L_2	L_3	L_4	L_5
A	117.8a	70.6de	48.6g	77.3de	119.3cd	--	178.5cd	208.6ab	--	174.2ab
B	78.3cd	150.6a	112.5ab	131.5ab	140.7abc	199.5b	192.4bcd	160.1bc	185.7a	143.8b
C	72.0cd	82.6de	86.3cde	157.0a	153.6a	--	153.2d	173.5bc	297.8a	151.8b
D	--	57.5e	52.9g	56.9e	93.9e	--	--	--	--	--
E	63.5cd	91.0cde	63.4efg	84.1de	141.6abc	--	181.2cd	--	--	191.8ab
F	82.3bcd	132.0abc	131.2a	145.1ab	151.8ab	212.8ab	249.6a	214.5ab	200.2a	221.7a
G	65.1cd	139.5ab	66.5efg	102.4cd	142.0abc	--	--	168.7bc	--	158.8b
H	--	54.9e	59.1fg	74.4de	94.0e	--	--	--	--	--
I	51.3d	123.1bcd	78.3def	75.4de	109.8de	--	150.7d	152.1c	153.0a	166.7b
J	94.3bc	155.9a	95.8bcd	118.5bc	116.5cd	188.0b	163.0cd	177.7bc	149.5a	147.9b
K	113.4ab	155.2a	54.7fg	78.1de	139.8abc	--	180.2cd	165.9bc	168.4a	191.6ab
L	80.0cd	120.8bcd	105.8bc	123.3bc	133.3bc	186.7b	203.9ab	208.6ab	181.8a	151.1b
M	66.4cd	137.5abc	115.2ab	133.1ab	125.9bc	247.0a	233.0ab	259.8a	194.3a	193.9a

Spray distribution

Spray deposition results at each sampling point are shown in Table 4. It can be seen that deposition in points B and J located at the left and right symmetrical positions next to the fuselage are the highest. Also in points L and M -located at the outer side depositions were relatively high, both for the stationary and hovering state. Compared with other sampling points, deposition of point F was also higher, and the deposition of points D and H was the lowest. Based on the installation position of the UAV nozzles (Fig 1 and Fig 2c), points B and J were located between two nozzles on the left and right sides of the fuselage with the closest distance from the nozzle. Point L, M and F were located in the middle area of the spray fans of the two nozzles.

For the sampling points further away from the nozzles (points D, H, E and G), the deposition measured with the UAV in hovering-state was close to that of the corresponding point in static condition. Although the sampling points were not directly below the nozzle and its spray fan, the droplets were prone to move circumferentially to the adjacent area under the guidance of the downwash airflow (Yang et al., 2018). Therefore, the deposition at sampling points near the nozzle in hovering-state was significantly higher than under static state, especially for the points B, J, L, M and F located in the middle of the spray fans. Nevertheless, differences in spray deposition between hovering and static state decreased further away from the UAV.

TABLE 4. Spray deposition (μL/cm²) on different measurement layers and sampling positions.

Sampling points	Static state					Hovering state				
	L_1	L_2	L_3	L_4	L_5	L_1	L_2	L_3	L_4	L_5
A	1.52	0.16	0.31	0.28	1.93	3.29	6.00	3.75	7.29	2.94
B	2.27	7.32	4.17	6.30	6.60	12.16	12.76	13.66	10.37	8.77
C	0.24	4.61	5.04	5.87	3.43	1.39	5.43	3.00	2.53	3.60
D	0.09	0.08	0.12	0.06	0.48	0.12	0.17	0.04	0.17	0.18
E	1.11	0.15	1.11	0.07	1.69	0.72	0.53	0.21	1.86	0.73
F	0.82	2.67	3.57	2.73	6.00	4.30	4.81	7.00	7.75	4.57
G	0.08	1.76	5.42	2.58	4.26	0.62	0.88	1.79	1.38	2.17
H	0.03	0.18	0.63	1.31	1.85	0.07	0.07	0.11	0.42	0.44
I	0.21	0.16	1.08	0.30	4.30	3.30	2.22	1.41	4.60	2.86
J	2.61	4.70	5.32	4.77	4.37	13.56	12.93	14.49	13.46	6.84
K	0.19	3.74	5.55	3.21	5.13	8.33	5.60	4.97	3.71	6.69
L	1.52	3.27	7.01	3.80	3.67	5.67	7.64	6.67	5.84	4.33
M	1.84	2.82	3.96	5.06	2.80	5.47	3.78	2.23	3.52	4.72

The average spray deposition, standard deviation and the *RSD* in each measurement layer and L-B-F-J-M section were calculated under the static-state and hovering-state spraying (Table 5). For the whole measurement layer, the average deposition and *RSD* of hovering state spray in L_1 layer was higher than that of static state, with an average deposition and *RSD* of 3.76 $\mu L/cm^2$ and 73.22% in hovering-state, and 0.88 $\mu L/cm^2$ and 159.57% in static-state. However, the effects of rotor airflow on droplet distribution diminished with the distance below the UAV. In layer L_5, the *RSD* of the static-state reduced to 79.25%, while the *RSD* of hovering-state reached up to 109.55%. The downwash airflow increased spray deposition in the measurement layers, but reduced the uniformity of deposition to some extent.

It could be seen from Table 4 that the droplets of the UAV spray were mainly concentrated near the L-B-F-J-M section, and the droplet distribution performance of this section mainly determines the spraying swath and spray uniformity. The results showed that due to the downwash airflow, a large number of droplets were deposited on this section, and the average deposition in hovering-state in all layers was greater than in static-state. Furthermore, the downwash airflow generated by the UAV rotors could also improve the uniformity of droplet distribution in this section. For the static-state spray, the *RSD* of deposition in L_1 layer was 89.31%, and the *RSD*s in layers L_2 to L_4 were about 60%. In contrast, the *RSD*s in hovering-state on layers L_1 to L_4 were about 50%. The best spray performance was found in L_5, with an average deposition and *RSD* of 4.69 $\mu L/cm^2$ and 51.81% in static-state, and 5.85 $\mu L/cm^2$ and 36.87% in hovering-state spray. The periphery spreading of the downwash airflow near the ground (Zhang et al., 2020a) improves the uniformity of droplet distribution in the L-B-F-J-M section.

TABLE 5. Average spray deposition ($\mu L/cm^2$), standard deviation ($\mu L/cm^2$) and relative standard deviation (%) of on whole measurement layers and L-B-F-J-M sections.

Measurement layers	Whole measurement layer						L-B-F-J-M section					
	Static state			Hovering state			Static state			Hovering state		
	AD	SD	RSD	AD	SD	RSD	AD	SD	RSD	AD	SD	RSD
L_1	0.88	1.41	159.57	3.76	2.75	73.22	1.81	1.62	89.31	8.42	4.17	49.48
L_2	2.43	2.65	108.78	4.84	4.23	87.46	4.16	2.49	59.96	8.06	4.27	53.00
L_3	3.33	3.36	100.76	4.56	4.86	106.52	4.81	2.85	59.33	8.81	4.82	54.76
L_4	2.79	2.87	102.60	4.62	4.54	98.18	4.53	2.77	61.08	8.19	4.16	50.77
L_5	3.58	2.84	79.25	4.51	4.94	109.55	4.69	2.43	51.81	5.85	2.16	36.87

Note: *AD*: average deposition; *SD*: standard deviation; *RSD*: relative standard deviation.

CONCLUSIONS

In this paper, the downwash airflow field of DJI MG-1P eight-rotor plant protection UAV in hovering and static state was measured with a 3D wind speed and direction anemograph, and the effects of rotor airflow on droplets velocity, particle size and spray deposition were analyzed. The main conclusions are as follows:

(1) The core area of the rotors downwash airflow field diffused and the intensity decreased with an increasing distance below the UAV. The maximum airflow speeds at distances of 50, 90, 130, 170 and 210 cm below the UAV were 9.24, 7.75, 6.95, 6.50 and 3.24 m/s, respectively.

(2) The direction of the airflow directly under the UAV was almost vertically downward and first increased and then decreased in speed. The velocity and direction of the downwash airflow on both sides of the UAV were symmetrically distributed with the shape of a horn that "shrinks first and expands later". The downwash airflow was directed outward with angles in the vertical direction of 71.3° and 81.5° at the height of 20 cm above the ground.

(3) Compared with the static-state spray, the high-speed downwash airflow in the hovering-state spray significantly increased droplet velocity and size, and droplet velocities are generally consistent with the airflow field intensity.

(4) The downwash airflow increased spray deposition in the measurement layers, but reduced the uniformity of the deposition to some extent. For the L-B-F-J-M section, which plays a decisive role of spraying swath and uniformity, the near ground deposition performance of the hovering-state spray was the best, with an average deposition and *RSD* of 5.85 $\mu L/cm^2$ and 36.87%.

ACKNOWLEDGMENTS

REFERENCES

Boukhalfa HH, Massinon M, Belhamra M, Lebeau F (2014) Contribution of spray droplet pinning fragmentation to canopy retention. Crop Protection 56:91-97.

Chen S, Lan Y, Bradley KF, Li J, Liu A, Mao Y (2017a) Effect of wind field below rotor on distribution of aerial spraying droplet deposition by using multi-rotor UAV. Transactions of the Chinese Society of Agricultural Machinery 48(8):105-113.

Chen S, Lan Y, Li J, Zhou Z, Liu A, Mao Y (2017b) Effect of wind field below unmanned helicopter on droplet deposition distribution of aerial spraying. International Journal of Agricultural and Biological Engineering 10(3): 67-77.

França JAL, Cunha JPR da, Antuniassi UR (2018) Spectrum and velocity of droplets of spray nozzles with and without air induction. Engenharia Agrícola 38: 232-237.

Giles DK, Billing RC (2015) Deployment and performance of a UAV for crop spraying. Chemical Engineering Transactions 44:307-312.

Hafeez A, Husain MA, Singh SP, Chauhan A, Khan MT, Kumar N, Chauhan A, Soni SK (2022) Implementation of drone technology for farm monitoring & pesticide spraying: A review. Information processing in Agriculture. https://doi.org/10.1016/j.inpa.2022.02.002

Herbst A, Bonds J, Wang Z, Zeng A, He X, Goff P (2020) The influence of Unmanned Agricultural Aircraft System design on spray drift. Journal of Cultivated Plants/Journal für Kulturpflanzen, 72(1):1-11.

Hu L, Zhou Z, Luo X, Wang P, Yan Y, Li J (2014) Development and experiment of a wireless wind speed sensor network measurement system for unmanned helicopter. Transactions of the Chinese Society for Agricultural Machinery 45(5):221-226.

International Organization for Standardization (2015) ISO 24253-1 Crop protection equipment - Spray deposition test for field crop. Geneva: ISO copyright office.

Kashdan JT, Shrimpton JS, Whybrew A (2007) A digital image analysis technique for quantitative characterisation of high-speed sprays. Optics and Lasers in Engineering 45(1): 106-115.

Kumar A, Rani M, Aishwarya, Kumar P (2022) Drone technology in sustainable agriculture: the future of farming is precision agriculture and mapping. Agriculture, Livestock Production and Aquaculture. Springer, Cham 2022: 3-12. https://doi.org/10.1007/978-3-030-93262-6_1

Lan Y, Chen S (2018) Current status and trends of plant protection UAV and its spraying technology in China. International Journal of Precision Agricultural Aviation 1(1):1-9. DOI: https://doi.org/10.33440/j.ijpaa.20180101.0002

Lan Y, Qian S, Chen S, Zhao Y, Deng X, Wang G, Zang Y, Wang J, Qiu X (2021) Influence of the downwash wind field of plant protection UAV on droplet deposition distribution characteristics at different flight heights. Agronomy 11(12): 2399.

Li J, Lan Y, Shi Y (2018) Research progress on airflow characteristics and field pesticide application system of rotary-wing UAV. Transactions of the CSAE 34(12): 104-118.

Li J, Shi Y, Lan Y, Guo S (2019) Vertical distribution and vortex structure of rotor wind field under the influence of rice canopy. Computers and Electronics in Agriculture 159: 140-146. https://doi.org/10.1016/j.compag.2019.02.027

Li X, Giles DK, Niederholzer FJ, Andaloro JT, Lang EB, Watson LJ (2021) Evaluation of an unmanned aerial vehicle as a new method of pesticide application for almond crop protection. Pest Management Science 77(1): 527-537. https://doi.org/10.1002/ps.6052

Nairn JJ, Forster WA (2014) Influence of spray formulation surface tension on spray droplet adhesion and shatter on hairy leaves. New Zealand Plant Protection 67: 278-283.

OECD (2021) Report on the state of the knowledge-literature review on unmanned aerial spray systems in agriculture, OECD Series on Pesticides, No. 105, OECD Publishing, Paris.

Pinguet B (2021) The role of drone technology in sustainable agriculture. Precision Ag. Available: https://www.precisionag.com/in-fieldtechnologies/drones-uavs/the-role-of-drone-technology-in-sustainable-agriculture/

Reitz RD, Bracco FV (1982) Mechanism of atomization of a liquid jet. Physics of Fluids 25: 1730-1742.

Shi Q, Liu D, Mao H, Shen B, Li M (2021) Wind-induced response of rice under the action of the downwash flow field of a multi-rotor UAV. Biosystems Engineering 203: 60-69.

Sun C, Liu C (2019) Construction and application of droplet canopy penetration model for air-assisted spraying pattern. Transactions of the Chinese Society of Agricultural Engineering 35(15): 25-32.

Tang Q, Zhang R, Chen L, Xu M, Yi T, Zhang B (2017) Droplets movement and deposition of an eight-rotor agricultural UAV in downwash flow field. International Journal of Agricultural and Biological Engineering 10(3):47-56.

Teske ME, Wachspress DA, Thistle HW (2018) Prediction of aerial spray release from UAVs. Transactions of the ASABE 61(3): 909-918.

Wang C, He X, Jane B, Qi P, Yang Y, Gao W (2020) Effect of downwash airflow field of 8-rotor unmanned aerial vehicle on spray deposition distribution characteristics under different flight parameters. Smart Agriculture 2(4): 124-136.

Wang C, He X, Wang X, Wang Z, Wang S, Li L, Bonds J, Herbst A, Wang Z (2018a) Testing method and distribution characteristics of spatial pesticide spraying deposition quality balance for unmanned aerial vehicle. International Journal of Agricultural and Biological Engineering 11(2): 18-26.

Wang S, Dorr GJ, Khashehchi MX, He X (2015) Performance of selected agricultural spray nozzles using particle image velocimetry. Journal of Agricultural Science and Technology 17 (3): 601–613.

Wang S, Liu Y, He X, Li Y, Song J, Liu Z, Ling Y (2018b) Distribution and residues of imidacloprid sprayed with electric multi-rotor unmanned aerial vehicle in paddy. International Agricultural Engineering Journal 27(1):53–63.

Wang S, Song J, He X, Li Y, Ling Y (2016) Design of air-assisted electric knapsack sprayer and experiment of its operation performance. Transactions of the Chinese Society of Agricultural Engineering 32(21): 67-73.

Weisensee PB, Tian J, Miljkovic N, King WP (2016) Water droplet impact on elastic superhydrophobic surfaces. Scientific reports 6(1): 1-9.

Xiahou B, Sun D, Song S, Dai Q (2020) Simulation and experimental research on droplet flow characteristics and deposition in airflow field. International Journal of Agricultural and Biological Engineering 13(6): 16-24.

Xiongkui H, Bonds J, Herbst A, Langenakens J (2017) Recent development of unmanned aerial vehicle for plant protection in East Asia. International Journal of Agricultural and Biological Engineering 10(3): 18-30. https://doi.org/10.3965/j.ijabe.20171003.3248

Yang F, Xue X, Cai C, Zhou Q (2018) Effect of down wash airflow in hover on droplet motion law for multi-rotor unmanned plant protection machine. Transactions of the Chinese Society of Agricultural Engineering 34(2):64-73.

Yang F, Xue X, Zhang L, Sun Z (2017) Numerical simulation and experimental verification on downwash air flow of six-rotor agricultural unmanned aerial vehicle in hover. International Journal of Agricultural and Biological Engineering 10(4):41-53.

Zhang H, Lan Y, Wen S, Xu T, Yu F (2020a) Research progress in rotor airflow model of plant protection UAV and droplet motion mechanism. Transactions of the Chinese Society of Agricultural Engineering 36(22):1-12.

Zhang H, Qi L, Wu Y, Musiu EM, Cheng Z, Wang P (2020b). Numerical simulation of airflow field from a six–rotor plant protection drone using lattice Boltzmann method. Biosystems Engineering 197:336-351. https://doi.org/10.1016/j.biosystemseng.2020.07.018

Zhang P, Zhang W, Sun H, Fu H, Liu J (2021) Effect of the downwash flow field of a single-rotor UAV on droplet velocity in sugarcane plant protection. Engenharia Agrícola 41: 235-244.

Zhang S, Xue X, Sun Z, Zhou L, Jin Y (2017) Downwash distribution of single-rotor unmanned agricultural helicopter on hovering state. International Journal of Agricultural and Biological Engineering 10(5):14-24.

Zwertvaegher IK, Verhaeghe M, Brusselman E, Verboven P, Lebeau F, Massinon M, Nuyttens D (2014) The impact and retention of spray droplets on a horizontal hydrophobic surface. Biosystems Engineering 126: 82-91.